2D Dopant Profiling Using Scanning Kelvin Probe Microscopy

Session O-7

Albert K. Henning, Todd Hochwitz
Thayer School of Engineering
Dartmouth College Hanover, NH 03755

Charles Daghlian
Rippel EM Facility Dartmouth College Hanover, NH 03755

James Slinkman, James Never
Phil Kaszuba, Steven Hoffmann†
IBM Microelectronics Essex Junction, VT 05452

Abstract

A simultaneous combination of scanning Kelvin probe and atomic force microscopy has been used to address the problem of profiling lateral dopant concentrations on a sub-micron scale in silicon microstructures. By measuring the potential difference which minimizes the electrostatic force between a probe and surface of a sample, we estimate the work function difference between the probe and surface. To the extent that this work function difference is a consequence of the dopant concentration near the sample surface, we infer doping profiles from our measurements. Our system has a lateral resolution better than 100 nm, and dopant profile measurements are obtained in ambient atmosphere. Structures examined and presented here include doped stripes and squares on silicon, and the first successful direct measurement of the lightly-doped drain of a metal-oxide-silicon field-effect transistor. Our measurements are compared to predictions based on two- and three-dimensional process and device simulation tools, which indicate our technique is sensitive to relative changes in dopant density from 10^{15} cm^{-3} to 10^{20} cm^{-3} with better than ten percent accuracy.

1 Introduction

Measurement of doping profiles in silicon and gallium arsenide (GaAs) devices on micron and sub-micron scales has long been a goal for process and device engineers. One-dimensional profile measurement has been available since the middle 1970's. However, in silicon bipolar, silicon metal-oxide-semiconductor field-effect transistors (MOSFETs), and GaAs-related heterostructure devices, accurate knowledge of two- and even three-dimensional profiles is required in order to predict device performance and reliability. Corroboration of process simulator predictions of heterostructure and doping profiles, with the actual profiles themselves, therefore becomes increasingly important as sub-micron dimensions are achieved in manufacturing practice.

†Current address Crowley's Ridge College, Paragould, Arkansas.

To be of greatest use to the electronic device and integrated circuit communities, measurement techniques should meet several milestones. Sample preparation should be minimal, and if possible non-destructive as well. Equipment cost should be relatively small. Measurement time should be short to yield high sample throughput. Techniques must have sufficient sensitivity to measure the full range of desired doping profiles. Viable techniques must also be sufficiently accurate in determining absolute dopant concentrations. Measurements must be repeatable, in that successive measurements on a sample may differ only slightly. Instrument design must be solid in order to ensure measurements are also reproducible, whether the probe tip, or some other instrument parameter, is changed.

The central goal of our work is to develop Scanning Kelvin Probe Microscope (SKPM) as a leading means to measure two-dimensional (2D) dopant concentration profiles. Our eventual goal is the measurement of doping profiles, with spatial XY resolution near 25 nm, and absolute dopant concentration accuracy of ten percent, over the full range of dopant densities important to semiconductor device design and fabrication. We require the measurement to be non-destructive, with minimal sample preparation, and rapid throughput, including any necessary data reduction. This paper reports our progress in achieving these ends.

Extensive reviews of most available profiling techniques, in one, two, and three dimensions, have been presented [1,2], and will not be repeated here. Techniques specific to 2D dopant profiling in silicon are important to our work, however, and are worth summarizing briefly.

Scanning Capacitance Microscopy (SCM) [3,4] is the leading 2D dopant profiling technique at this time. Sample preparation is minimal. Plan-view measurements are non-destructive, while cross-sectional measurements require scribing and breaking the sample. Measurements are taken in air. Lateral resolution is limited to twice the probe tip radius, roughly 100 nm at present. Dopant concentrations may be imaged in the 10^{16} cm$^{-3} - 10^{21}$ cm^{-3} range. Accuracy is sufficient to allow comparison with numerical process simulation tools, though as yet insufficient to allow distinction between subtle changes in dopant diffusion models. A single sample suffices to obtain an entire profile. Computer data deconvolution is required. Improvements in accuracy will require calibration against well-defined experimental matrices, yielding samples with doping profiles well-characterized by more traditional means.

Secondary-ion mass spectrometry (SIMS) has been used in conjunction with samples beveled on multiple angles [5,6], or etched in vertical relief at an angle to an implanted edge [7]. Analysis proceeds using computer tomographic techniques. The technique is destructive,

time-consuming, and requires multiple samples to achieve a single profile, but is otherwise successful in meeting many of the 2D dopant profiling goals.

Spreading resistance combined with mechanical magnification using angled and beveled etching has recently achieved $10^{12} - 10^{19}$ cm^{-3} sensitivity with 25-50 nm lateral spatial resolution [8]. Computer deconvolution of the data is required.

An optical technique has been successful in detailing profiles in the $10^{14} - 10^{19}$ cm^{-3} range, with lateral resolution of 40 nm [9]. Relatively time-consuming sample etching and beveling is required. Multiple samples are required, one for each isoconcentration line in the profile.

Atomic Force Microscopy combined with controlled etching has been used with some success to decorate dopant profiles [10]. Control of the etch solutions, and calibration of etch rates against sample with well-known dopant concentrations, have yet to be established.

2D profiles have been inferred using a coupling between simulation, and electrical measurement of source-drain overlap capacitance in a MOSFET [11, 12]. The interplay between simulation and measurement can be tedious, and subject to the specifics of the simulation transport and capacitance models. Additional test structures to obtain, for instance, gate-to-drain overlap capacitances, must be fabricated and measured. The technique is nondestructive, and requires a single sample to obtain profile data, but is specific to the MOSFET structure, making generalization to other structures problematic.

Previous experimental results have shown that simultaneous use of a Scanning Atomic Force Microscope (AFM) and SKPM can provide qualitative dopant concentration profiles [13–17]. In this work we attempt to lay the foundation for determining a quantitative relationship between measurements obtained through the use of SKPM and the theoretical 2D dopant profiles in silicon microsctructures. Compared to the previous methods outlined above, we believe this technique offers the best means to achieve our goals. To date, our lateral XY positional precision is regularly 50 nm; we have achieved 15-25 nm with some care. Our vertical Z positional resolution is ≈ 1 nm in AFM mode. In SKPM mode, we have achieved a measurement sensitivity of 1 mV/$\sqrt{\text{Hz}}$, which translates at our measurement frequencies to a resolution of roughly 5 mV. We believe a resolution of 0.5 mV is achievable. Such resolution in the measured electrochemical potential difference (EPD) between tip and surface yields easily the sensitivity to distinguish dopant concentration changes over the 10^{15} cm$^{-3} - 10^{20}$ cm^{-3} range. Due to probe tip geometry, signal convolution between tip and surface, and masking effects at the surface, we are only able to infer changes in dopant concentration with a lateral resolution of 50 nm to 100 nm. Our present technique will require calibration to known dopant concentration standards, or advances in understanding and control of the probe tip/sample surface system, in order to achieve our desired absolute accuracy.

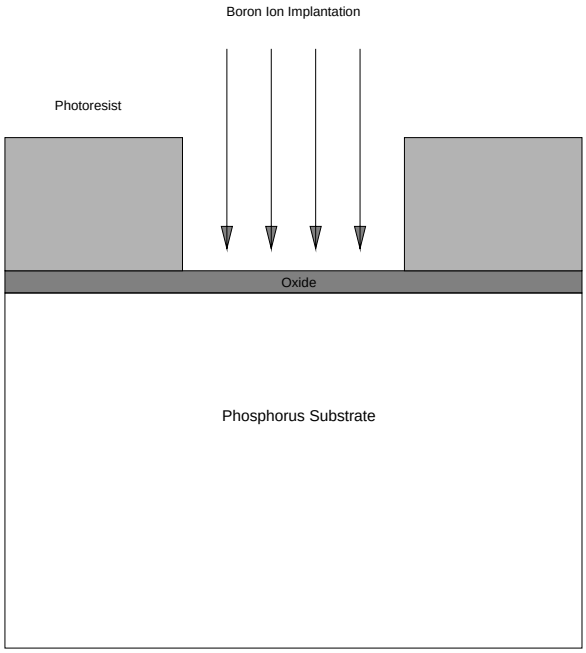

Figure 1: Cross-section schematic of dopant implant experiments undertaken in this work.

2 Experiments

Our SKPM is a non-contact AFM built at IBM – Yorktown Heights, to which we have added the necessary hardware for implementing the Kelvin measurement technique [18]. The unit is currently on loan to Dartmouth College from IBM – Essex Junction. The system occupies a 100 ft^2 room, which is ample for holding all elements of the system and support equipment. The deflection of a force sensing cantilever is detected with a heterodyne-based interferometer [19]. The heterodyne system allows us to monitor the deflection of the cantilever simultaneously at several different frequencies. One frequency is used for the force gradient loop, another for the Kelvin loop [20]. The harmonic of the Kelvin excitation frequency is used to obtain the $\frac{\partial C}{\partial z}$ signal. We are able to locate several peaks in the frequency response of the cantilever's deflection for operational use since it behaves as a lumped mass system. The system is described more fully in [21,22].

Figure 1 shows a cross-section of the general structure for most of our experimental measurements to date. The fabrication sequence is given in Table I. In essence, we fabricated 2.5 μm by 2.5 μm contact holes in SiO_2, and implanted boron into these holes, on n-type (phospho-

rus) substrates. These samples were fabricated at IBM–Essex Junction.

Table I: Experimental process flow used in structure fabrication and simulation.

Step	Process Information
Start	Phosphorus-doped (100) silicon, 20-40 Ω-cm, 125 mm diameter
Clean	Standard RCA-type clean
Oxidation	22 nm MOS gate-quality thermal oxide
Photolithography	Mask contact holes
Ion Implantation	Boron, 10^{15} cm^{-2}, 25keV
Oxide etch	Etch oxide in contact holes
Strip Photoresist	Plasma O_2
Anneal	O_2, 5-10-5 min., dry-wet-dry, 900 C
Oxide etch	Wet oxide etch, 100:1 DI:HF, 1 min.

After the final oxide etch, the samples were mounted on our microscope stage, and measured using the combination AFM/SKPM system we have built. Each scan required approximately thirty minutes. Note that the final oxide etch does not remove all the grown oxide, thus preserving the high-quality, low surface charge nature of the Si-SiO_2 interface.

We have also performed SKPM and AFM measurements on a MOSFET. The particular device measured was fabricated using a lightly-doped drain (LDD) technology [23]. To our knowledge, no technique has yet been successful in imaging the LDD doping profile of a MOSFET. We attempted to measure such a structure, though from the surface and not in cross-section, in order to validate our technique using a problem of high technological interest.

3 Results

The three-dimensional nature of the contacts is depicted in Figure 2, a FIELDAY [24] simulation. The actual contacts have corners which are more rounded than shown here, due to photolithographic effects at contact corners. The figure is useful for purposes of illustration, and subsequent comparison between the measured EPD and simulated work function difference (WFD).

Figure 3 shows a one-dimensional SIMS measurement of the vertical Z doping profile. The measurement was taken in a large implanted area, given the nature of the SIMS technique. It was used to corroborate the vertical doping profile found via SUPREM-IV [25] simulation.

A comparison of the normalized, one-dimensional, lateral XY signals from the Kelvin and AFM modes is given in Figure 4. The maximum Kelvin signal is 371 mV, while the maximum AFM signal corresponds to a height

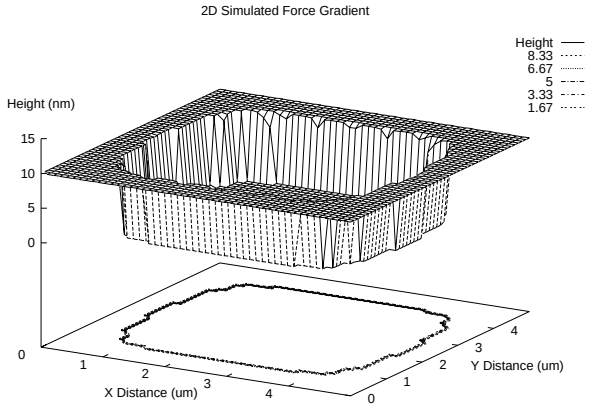

Figure 2: Three-dimensional view of 2.5μm $\times$ 2.5μm contact structure (simulated).

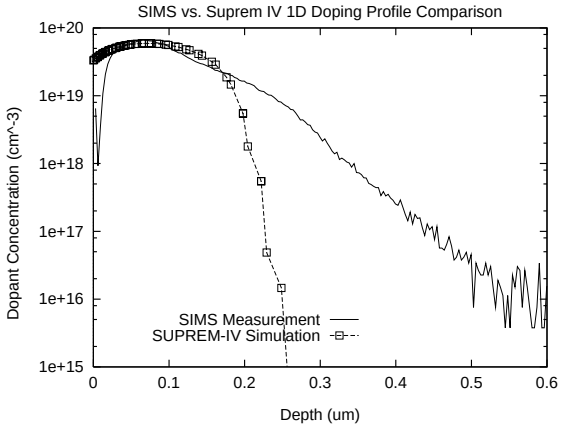

Figure 3: Comparison of (1D) SIMS-determined and SUPREM-IV dopant density profiles in the vertical Z direction.

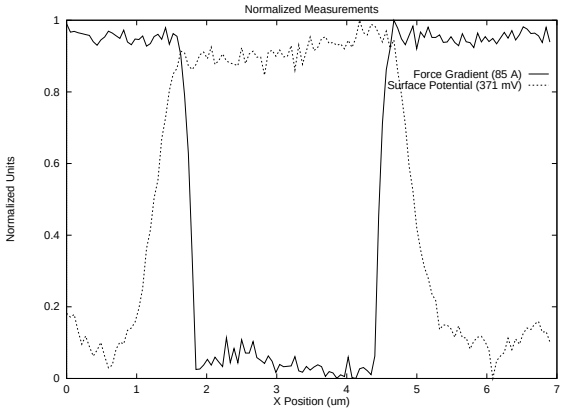

Figure 4: Normalized measurements (1D) of the lateral SKPM and AFM signals taken along a line cutting through the center of the contact.

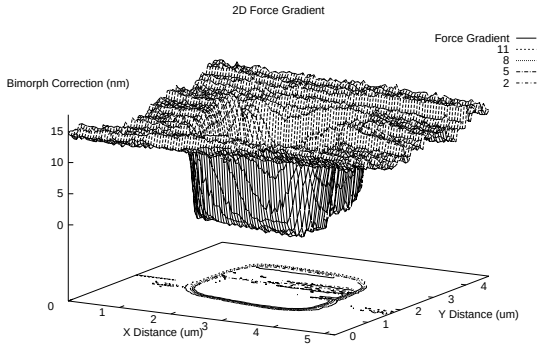

Figure 5: Contours of AFM measurement of 2D surface force gradient contours.

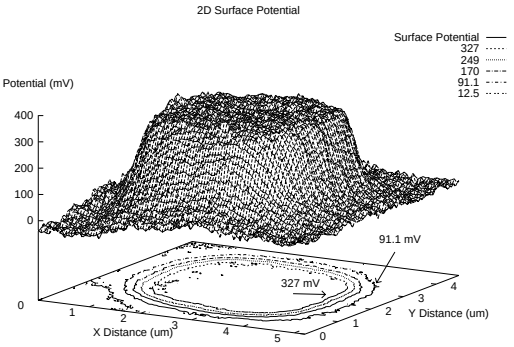

Figure 6: Contours of SKPM measurements of 2D, lateral XY tip-to-surface electrochemical potential difference.

of 8.5 nm. The measurement is taken along a line cutting through the center of the contact surface.

The AFM results from Figure 4 are collected for all scan lines of a single contact, and shown in contour form in Figure 5; Figure 6 shows the SKPM measurements of 2D U_{DC} contours, obtained simultaneously.

The schematic of the LDD MOSFET structure can be seen in Figure 7. Greyscale images of the AFM and SKPM signals obtained from this structure are shown in Figures 8 and 9.

We note that these measurements, of the XY dependence of force gradient and EPD (U_{DC}), are repeatable. Offsetting the scan window by half a frame shows the common portion of two successive images to be the same.

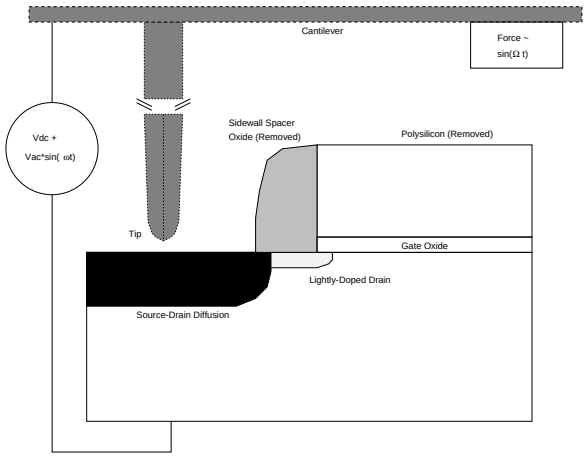

Figure 7: Schematic of the tip-surface system, including both atomic force and Kelvin modes. The frequency for the AFM measurement is Ω, while the frequency for the SKPM measurement is ω.

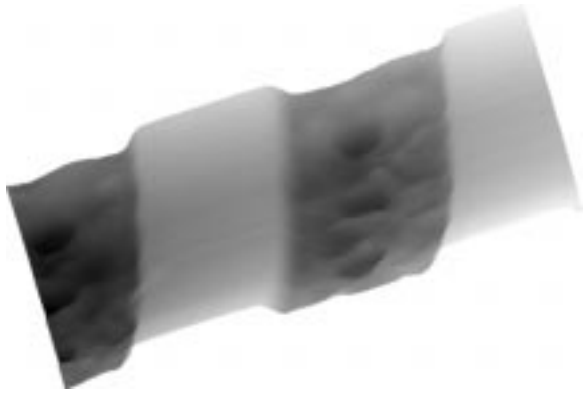

Figure 8: AFM surface image of source-drain and channels regions in an N-channel MOSFET.

Figure 9: SKPM image of source-drain and channels regions in an N-channel MOSFET. Note the clear delineation of the change from the heavily-doped to the lightly-doped region.

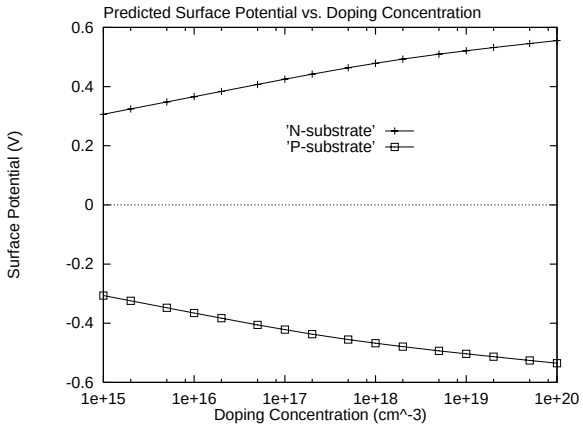

Figure 10: Relationship between expected tip-to-surface work function difference and substrate doping [based on Equations (1)-(3).

4 Discussion

In SKPM mode, an ability to resolve 1 mV changes in U_{DC} should translate to an estimated sensitivity to changes in actual dopant concentration of +/- 5% in the vicinity of 10^{14} cm^{-3}, and +/- 8% in the vicinity of 10^{18} cm^{-3}. This estimate is determined as follows. If the tip is taken to be undoped silicon, then the EPD applied to the tip, relative to the electrically-grounded, doped substrate, necessary to null the electrostatic field is:

$$U_{DC} = (E_C - E_F)_{tip} - (E_C - E_F)_{substrate} \qquad (1)$$

For acceptor doping only, and assuming the electron density has negligible impact on the determination of the Fermi level, Equation (1) becomes:

$$U_{DC} = \frac{E_g}{2} + \frac{kT}{2}\ln(N_C/N_V) - kT\ln\left[\frac{-1+\sqrt{1+16\,(N_A/N_V)\exp[E_a/kT]}}{8\exp[E_a/kT]}\right] \qquad (2)$$

Similarly, for donor doping only, and assuming the hole density has negligible impact:

$$U_{DC} = \frac{E_g}{2} + \frac{kT}{2}\ln(N_C/N_V) - kT\ln\left[\frac{-1+\sqrt{1+8\,(N_D/N_C)\exp[E_d/kT]}}{4\exp[E_d/kT]}\right] \qquad (3)$$

Inclusion of both free carrier types was found to cause at most a five percent change from the values determined using these simple formulas. The values of N_C and N_V used are 2.9×10^{19} cm^{-3} and 1.1×10^{19} cm^{-3}, respectively, and E_g is taken to be 1.12 eV at 300 K.

These expressions assume Fermi statistics, and that the silicon sample being measured is non-degenerate. The effect of band gap narrowing on work function is ignored. Impurity ionization energies E_a and E_d of 44 meV for both boron and phosphorus are assumed. Room temperature is presumed. A band picture (to estimate WFD from the SKPM probe voltage, U_{DC}, which minimizes the electrostatic force between probe tip and doped silicon surface) is also central to these expressions [22]. Note that exponential increases in dopant concentration lead to roughly linear increases in WFD and U_{DC}, so that relative accuracy should be roughly constant over a wide range of dopant concentrations.

The results of these equations are shown in Figure 10, which shows the relationship between the estimated WFD, based on the model of Equations (1-3), and substrate doping. Note that the curves will shift uniformly up or down in potential, if the work function of the tip is altered by deposition of gold, for instance; or, if the tip is not undoped silicon as in these calculations.

We have taken two tracks in the attempt to quantify doping profiles from our SKPM measurements. The first predicts the lateral surface doping profile in our contact structures using a process simulator, then applies Equations (1-3) to this doping profile to extract a predicted WFD. We proceed by validating the predicted vertical doping profile through comparison against a more traditional SIMS measurement. Figure 3 made this comparison of (1D) SIMS-determined, and SUPREM-IV [25] doping profiles in the vertical Z direction. Care was taken in the SUPREM-IV simulation to reproduce the actual implant sequence, which included four, seven degree angled implants, directed in effect at each of the four contact sides. The discrepancy between the SIMS and SUPREM-IV profiles in the tail region is relatively unimportant,

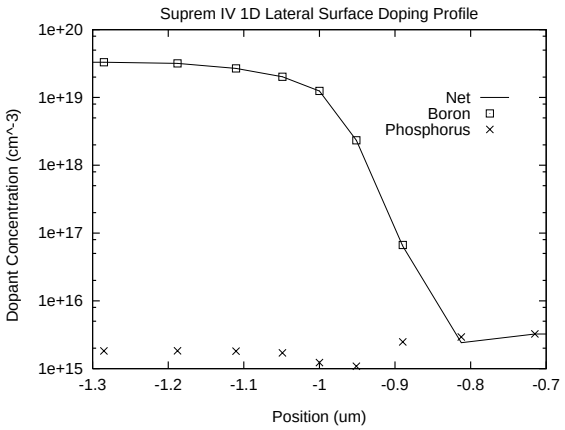

Figure 11: SUPREM-IV simulation of (1D) lateral XY surface dopant profile, taken along a section through the contact center.

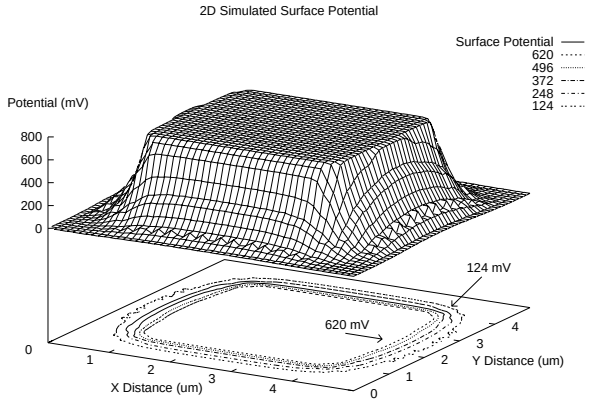

Figure 13: Two-dimensional contours of predicted tip-to-surface work function difference, based on FIELDAY simulation using Gaussian-derived dopant profiles.

since lateral diffusion should depend little on such low concentrations. The discrepancy between measured and simulated doping nearest the surface, however, causes us greater concern. We are working to adjust the SUPREM-IV parameters, to match the measured profile more fully. We then use the lateral XY surface doping profile from the same simulation, taken along a section through the contact center and shown in Figure 11. These doping values combine with Equations (1-3) to predict tip-to-surface WFD.

The results of this procedure are shown in Figure 12, where comparison is also made to the measured (1D) SKPM EPD. The predicted WFD changes too sharply, and has a greater spread from maximum to minimum value. From this comparison, we draw two important conclusions. First, screening effects reduce the magnitude of our measured signal versus the ideal. Second, the 'softness' in the transition from the boron to the phosphorus regions indicates the non-point nature of our measurements. Either the measured signal at XY, or the actual surface work function at XY, is derived from contributions beyond XY.

In order to explore this issue further, in the second track we used *ad hoc* Gaussian-based doping profiles in a FIELDAY [24] simulation of our tip-surface system, in order to predict the WFD expected from the given profile. The results, in Figure 13, can be compared to the FIEL-

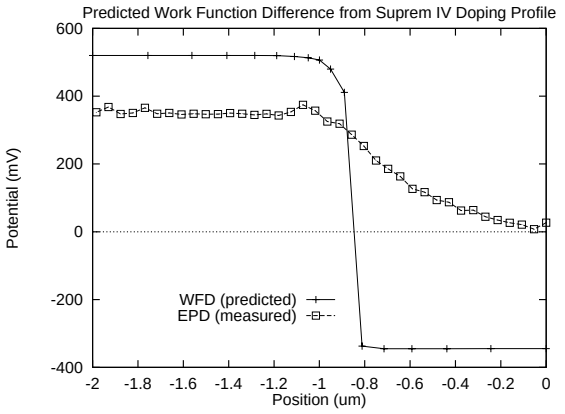

Figure 12: Comparison of measured SKPM (1D) tip-to-surface electrochemical potential difference, taken along a section through the contact center, with predicted (1D) U_{DC} derived from Equation 1 and Figure 11

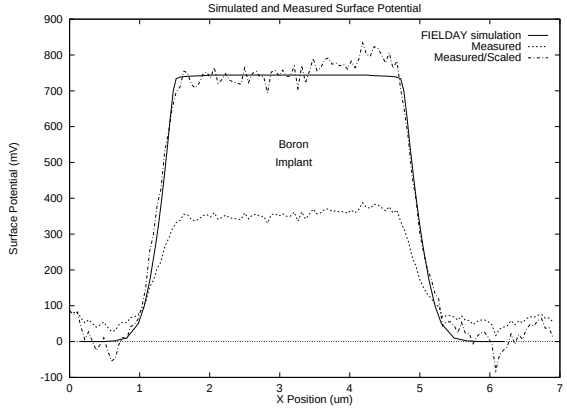

Figure 14: One-dimensional SKPM scan through contact center, before and after scaling of measured potential, compared with predicted (1D) tip-to-surface work function difference derived from the FIELDAY simulation shown in Figure 13.

DAY topography of Figure 2, in the same manner that the measurements in Figures 5 and 6 are compared. Qualitatively, the simulated WFD has more widely-spaced contours compared to the topography, just as we observe experimentally. In fact, the use of a numerical solution to find the WFD from the doping profile succeeds in predicting the spatial extent of the profiles, where the simple application of Equations (1-3) fails (see Figure 14). Quantitatively, however, the predicted WFD and measured EPD magnitudes still differ by an apparent scaling factor (see further discussion below).

We remark once more that one of our goals is to measure true lateral doping profiles to improve models of lateral and vertical diffusion. Given the uncertainty in the literature of lateral dopant diffusion models, we recognize a prediction of lateral doping profile will not necessarily be valid, simply because the SIMS and SUPREM-IV profiles compare well. However, it will serve as a point of departure for the sake of qualitative comparison.

From these two attempts, it is clear that neither the simple estimate represented by the model of Equations (1-3), nor an estimate based on the numerical solution of Poisson's equation, offers the opportunity for absolute determination of the dopant concentration, through an exact equation of estimated WFD and measured EPD.

However, a relative determination can be made. The comparisons in both Figures 11 and 12 show we are able to determine relative dopant concentrations with more than sifficient sensitivity. If the maximum value of the measured EPD, shown in Figures 4, 5, and 6 corresponds to the maximum surface dopant concentration predicted by SUPREM-IV (or used in the FIELDAY simulation); and if the minimum value of the measured EPD similarly corresponds to the minimum dopant concentration prediction; then 1 mV changes in our surface electrochemical potential measurements are related to eight percent changes in dopant concentration. This sensivity is within our ten percent goal.

With respect to our LDD measurements, Figures 8 and 9 clearly show the transition between the heavily doped drain implant region and the LDD structure. The LDD doping profile penetrates beneath the polysilicon gate and sidewall oxides spacer regions, as expected from the drive-in cycles experienced after implant. In Figure 8, the dark bands are the source-drain regions. The three dark circular structures are the result of tungsten contacts to this diffusion region. The widths of the drain-source and lighter-contrasted channel regions are 1 μm. Comparing Figures 8 and 9, we see that the AFM image of the source-drain diffusion area has the same width as the SKPM-imaged, heavily-doped portion of the region. However, we also see the encroachment of the more lightly-contrasted LDD region into the device channel in Figure 9. This is consistent with expectations from the processing of these devices, and highlights the new information which SKPM makes available to process and device engineers.

The measurements shown here are only a small fraction of those we have taken. Dopants implanted into arrays of contact holes and stripes, for substrates of both polarities, have been imaged with consistent interpretation.

Clearly, however, we have only achieved part of our goal. In order to determine absolute dopant concentration from our measurements, we need to make advances in a number of areas. These are discussed as follows:

4.1 Tip and Microprobe Geometry

Ideally we would use a "dual-resonance" cantilever in order to get two distinct, and very strong, resonant peaks, at ω and Ω. Such a cantilever can be constructed using two discrete widths on the lever arm leading to the probe tip. This would increase our sensitivity particularly in SKPM mode, since the mechanical resonance at the SKPM frequency ω is not nearly as strong as at the fundamental AFM frequency Ω. Pending incorporation of such tips, we must excite our uniformly shaped cantilever at the two best frequencies available.

We have demonstrated the reproducibility of our technique through measurements on a single contact sample, using both sharp (radius = 5 nm) and dull (radius = 100 nm) tips, over a two month period, with acceptably comparable results. With both sharp and dull tips, 300 mV peak-to-peak measurement swings were obtained on the same samples discussed in this work. Reversing the polarities of the tip-sample electrical connections (that is, grounding the tip *vs.* grounding the sample) changed the signal contrast, but not the peak-to-peak swing. Using a new, sharp tip, however, requires a large value for V_{ac}. Once the tip dulls, the value of V_{ac} required drops considerably (by as much as a factor of ten). Equation (5) allows us to determine what is happening. For a particular material (with the Kelvin loop unlocked), V_{DC} (or U_{DC}) is fixed. The only causes for change in the measured force are the amplitude of the *ac* component to the Kelvin signal V_{ac}, and the value of $\frac{\partial C}{\partial z}$. When the tip dulls, $\frac{\partial C}{\partial z}$ increases. Once $\frac{\partial C}{\partial z}$ goes up, the value of V_{ac} required to yield the same detected force drops. If the tip is sharp, $\frac{\partial C}{\partial z}$ is small and V_{ac} must increase to yield the same detectable force.

4.2 Effects of Surface Physics

Dopant profiling has been done on GaAs samples, using STM in ultra-high vacuum [26]. Success with GaAs would seem to encourage application of this technique to silicon. However, the needs for a high vacuum, and for a conductive substrate, compromise our goals of speed, and ease of measurement and sample preparation. Furthermore, it has been shown that high-vacuum STM of doped silicon

surfaces is unable to image dopant concentration, due to the collapse of the silicon band gap at the surface of an ultra-clean, cleaved silicon sample. Attempts to resolve this situation using H_2 to passivate the surface have been unsuccessful [27].

We believe our measurements succeed, where the high-vacuum STM measurements fail, because of the presence of a passivating, high-quality surface oxide. Our sample preparation protocol (see Table I) etches away the top 5-10 nm of SiO_2, thus removing any charged surface contaminants. The remaining oxide, grown under stringent purity requirements, will have low charge densities. The presence of an oxide does imply the possible presence of charged interface states or fixed oxide charges, even under the best of growth conditions. Previous work explored the effect of surface states on the vibrating reed Kelvin probe measurement, applied to amorphous silicon thin film growth [28]. The large density of mid-gap states in the bulk material, characteristic of amorphous silicon, makes direct comparison to our sample system unwarranted. Nonetheless, we can still estimate the effect of charged surface states (or, if our samples are protected by thin thermal or native oxides, the effect of fixed oxide charge) in the following way. Charged surface states or fixed oxide charge will shift the flatband voltage of the tip-sample capacitor, and our Kelvin measurement, by an amount:

$$\Delta V_{flatband} = \Delta U_{DC} = q\frac{N_F\, t_{ins}}{\epsilon_{ins}} \qquad (4)$$

where N_F is the surface charge density in cm^{-2}, t_{ins} is the thickness of the dielectric separating the tip and sample, and ϵ_{ins} is the dielectric constant. Presuming a dielectric of silicon dioxide, 10 nm thick, the flatband shift will be 4.7 mV for $N_F = 10^{10}$, and 47 mV for $N_F = 10^{11}$. Most thermal oxides fabricated using modern technology, on light-to-moderately doped substrates, will have N_F values easily in, or even below, this range. Minimization of the change in the Kelvin signal caused by surface charge can thus be minimized by decreasing the charge density through alternative hydrogen passivation methods [29–31], decreasing the tip-to-surface distance, or increasing the dielectric constant of the region separating the tip and surface. We are exploring each of these options, but clearly, the issue of surface charge commands our attention.

Our simple analysis in Equations (1-3) presumes a uniformly doped surface. Yet, the electrostatic force acting on a microprobe tip in the vicinity of a $p-n$ junction has an inhomogeneous character which will likely alter the interpretation of results in the vicinity of such a surface junction. We are presently exploring these effects, using analytical and numerical simulation means.

We have observed the spatial and temporal effects of surface charges in our SKPM measurements, as moderate changes in the value of U_{DC} which must be applied to minimize the electrostatic force, and the cantilever resonance at frequency ω. Surface charges can be fixed spatially, as in charge trapped in an oxide [32]. Or, they can accumulate over the time scale of the SKPM scan, due to local variations in the measurement environment, which can accumulate charge on the tip. These variations may be caused by humidity [33], adsorption of air-borne particles, and related causes. We believe the environmental contributions to charging can be controlled, through improving the air and humidity control in the lab.

4.3 Calibration Using Known Standards

Ideally, regardless of tip geometry, surface effects, or environmental effects, a given sample's dopant concentration can be extracted from the SKPM measurement with consistent accuracy. For this goal to be achieved, calibration must be done. Calibration is not uncommon in the measurement of 2D doping profiles. 1D SIMS profiles, for instance, have been used to calibrate 2D isocentration contours highlighted using wet etching under UV illumination and SEM imaging [34].

Knowledge of the work function of the tip is critical to extraction of the dopant concentration. Furthermore, understanding the relationship between our tip-to-surface EPD measurements, and the doping and the surface beneath the tip, must provide the foundation of a quantitative SKPM technique. Toward this end, we are using SKPM to measure surfaces of samples with known dopant concentration over a wide XY area. These measurements will provide information to establish a quantitative relationship between dopant concentration and measured EPD. They will also allow controlled studies of the effects of surface preparation, and surface atmosphere during measurement.

4.4 Lateral Extent of Electrostatic Force

Our analysis of the SKPM technique is predicated on minimizing the electrostatic force between tip and substrate. To date, our analysis has considered Z effects only. However, our primary tip does not always have the atomically sharp character necessary for our Z-only analysis to be most valid. The electric field lines connecting the tip (especially a dull tip) to the substrate will have a lateral XY character, which needs to be considered. This can best be done by modifying the electrostatic force to be $\mathbf{F} = \nabla E$, where $\mathbf{F}$ is now a vector force, and E is the scalar, but now XYZ dependent, electrostatic energy.

Our analysis has also presumed charge neutrality at the substrate surface, in order to determine the the Fermi level. However, in these experiments we scan across a $p-n$ junction, which by nature includes a depletion region, which is not charge neutral. Taking this into consideration will be necessary in order to determine the absolute

doping concentration.

The overall result of quantitative consideration of these factors may lead to a simple scaling relation between the measured EPD, and the WFD estimated from it. Comparison between theoretical values for the WFD and our measurements of dopant profiles have shown a consistent scaling factor of 2.5 +/- 0.1 to date. That is, after first removing a constant offset, multiplying the measured SKPM signal by this scaling factor leads to very close agreement between simulated and estimated doping profiles. An example is shown in Figure 14, where the measured SKPM signal U_{DC} has been scaled by 2.46. The scaled EPD is compared to the WFD predicted for the given structure by FIELDAY. The lateral dimensions for the measured signal are tied to the surface force gradient changes attendant to the topographic changes of the contact edge, which are also matched to the FIELDAY result. This scaling factor is unrelated to the electronics in the SKPM feedback, but is at this juncture an empirical, yet successful, manipulation of our data.

5 Conclusions

We have demonstrated the application of the SKPM technique to the problem of determining dopant concentration profiles in two dimensions, at size scales below 100 nm. The technique is presently sensitive to changes in dopant concentration, from $\approx 10^{15}$ cm^{-3} to 10^{20} cm^{-3}, of less than ten percent at these size scales. Measurements are fast, and require little if any sample preparation. They are repeatable, and reproducible to the extent that changes in probe tip do not affect the measurements significantly. Calibration of our measurements against absolute dopant concentration standards remains to be demonstrated. The technique has been applied successfully to the imaging of relative doping profiles in micron-scale contact holes. It has also been used to image the technologically significant surface doping profile of the LDD region of a MOSFET. To our knowledge, this represents the first successful imaging of the LDD region by direct means. A simple equation between the measured electrochemical potential difference between the probe tip and sample surface, and the dopant concentration related work function difference, does not suffice to establish an absolute extraction of the doping profile. Predictions of the work function difference derived from two-dimensional process simulations yield good agreement, within a reproducible scaling factor. The origin of the scaling factor may be due to surface physics effects, and is one subject of our continuing investigations.

6 Acknowledgments

The authors acknowledge the following sources with gratitude: P. Cadrecha and the management of IBM-Essex Junction, for equipment and personnel support; research support (for TH and AKH) through an IBM Shared University Research Grant, an Analog Devices (Inc.) Career Development Professorship, and Thayer School funds; C. Levey for fabrication of the SiO_2 calibration samples; M. O'Boyle of IBM-Yorktown Heights for assistance in adding the Kelvin measurement capabilities to our scanning force microscope; and D. Antoniadis of the Microsystems Technology Laboratory at MIT for support provided during a sabbatical leave (by AKH) involving this work.

References

[1] C. Hill, in *Proc. Euro. Sol. St. Dev. Res. Conf.* (Adam Hilger, Bristol, UK, 1990), pp. 53–60.

[2] R. Subrahmanyan, J. Vac. Sci. Tech. **B10**, 358 (1992).

[3] J. A. Slinkman, C. C. Williams, D. W. Abraham, and H. K. Wickramasinghe, in *IEDM Proceedings* (IEEE Press, Piscataway, NJ, 1990), pp. 73–76.

[4] C. C. Williams, J. Slinkman, W. P. Hough, and H. K. Wickramasinghe, Appl. Phys. Lett. **55**, 1662 (1989).

[5] S. H. Goodwin-Johansson, M. Ray, Y. Kim, and H. Z. Massoud, J. Vac. Sci. Tech. **B10**, 369 (1992).

[6] S. H. Goodwin-Johansson, R. Subrahmanyan, C. E. Floyd, and H. Z. Massoud, IEEE Trans. Comp.-Aided Des. **TCAD-8**, 323 (1989).

[7] M. G. Dowsett and G. A. Cooke, J. Vac. Sci. Tech. **B10**, 353 (1992).

[8] T. Takigami and M. Tanimoto, Appl. Phys. Lett. **58**, 2288 (1991).

[9] R. Subrahmanyan, H. Z. Massoud, and R. B. Fair, J. Electrochem. Soc. **137**, 1573 (1990).

[10] V. Raineri, V. Privitera, W. Vandervorst, L. Hellemans, and J. Snauwaert, Appl. Phys. Lett. **64**, 354 (1994).

[11] N. Khalil and J. Faricelli, in *Proc. Simulation of Semic. Devices and Processes (SISDEP)* (Springer-Verlag, Berlin, 1993), p. 365.

[12] C. F. Machala, J. H. Chern, J. L. Wise, and P. Yang, Texas Instruments Tech. Jour. **11**, 22 (1994).

[13] Y. Martin, D. W. Abraham, and H. K. Wickramasinghe, Appl. Phys. Lett. **52**, 1103 (1988).

[14] D. W. Abraham, C. Williams, J. Slinkman, and H. K. Wickramasinghe, J. Vac. Sci. Technol. B **9**, 703 (1991).

[15] J. M. R. Weaver and D. W. Abraham, J. Vac. Sci. Technol. B **9**, 1559 (1991).

[16] J. M. R. Weaver and H. K. Wickramasinghe, J. Vac. Sci. Technol. B **9**, 1562 (1991).

[17] M. Nonnenmacher, M. O'Boyle, and H. K. Wickramasinghe, Ultramicroscopy **42–44**, 268 (1992).

[18] L. Kelvin, Phil. Mag. **46**, 82 (1898).

[19] Y. Martin, C. C. Williams, and H. K. Wickramasinghe, J. Appl. Phys. **61**, 4723 (1987).

[20] M. Nonnenmacher, M. P. O'Boyle, and H. K. Wickramasinghe, Appl. Phys. Lett. **58**, 2921 (1991).

[21] T. Hochwitz *et al.*, in *Proc. IBM Failure Analysis Conference* (PUBLISHER, ADDRESS, 1994).

[22] A. K. Henning, T. Hochwitz, J. Slinkman, J. Never, S. Hoffman, P. Kaszuba, and C. Daghlian, submitted to J. Appl. Phys. (unpublished).

[23] S. Ogura, P. J. Tsang, W. W. Walker, D. L. Critchlow, and J. F. Shepard, IEEE Trans. Elec. Dev. **ED-27**, 1359 (1980).

[24] K. A. Salsburg, P. E. Cottrell, and E. M. Buturla, in *Proc. NATO Adv. Study Inst., Process and Device Sim. for MOS-VLSI Circuits* (Martinus Nijhoff, The Hague, Netherlands, 1983), pp. 582–619.

[25] M. E. Law, C. S. Rafferty, and R. W. Dutton, SUPREM-IV User's Manual, Stanford (U.) Electronics Lab Technical Report (1989).

[26] M. B. Johnson, O. Albrektsen, R. M. Feenstra, and H. W. M. Salemink, Appl. Phys. Lett. **63**, 2923 (1993).

[27] C. K. Shih, private communication (unpublished).

[28] J. K. Arch and S. J. Fonash, J. Appl. Phys. **68**, 591 (1990).

[29] L. Tsau, D. Wang, and K. L. Wang, Appl. Phys. Lett. **64**, 2113 (1994).

[30] K. Usuda, H. Kanaya, K. Yamada, T. Sato, T. Sueyoshi, and M. Iwatsuki, Appl. Phys. Lett. **64**, 3240 (1994).

[31] E. S. Snow and P. M. Campbell, Appl. Phys. Lett. **64**, 1932 (1994).

[32] T. Hochwitz, A. K. Henning, C. Daghlian, and J. Slinkman (unpublished).

[33] T. Thundat, R. J. Warmack, G. Y. Chen, and D. P. Allison, Appl. Phys. Lett. **64**, 2894 (1994).

[34] L. Gong, A. Barthel, J. Lorenz, and H. Ryssel, in *Proc. Euro. Sol. St. Dev. Res. Conf.* (Springer-Verlag, Berlin, 1989), pp. 198–201.